

NUMERICAL AND EXPERIMENTAL INVESTIGATION OF THE BURST RESISTANCE OF GLASS-FIBER THERMOPLASTIC COMPOSITE PIPES UNDER INTERNAL PRESSURE

L. Yao,¹ Sh. Wang,^{2,3*} X. Meng,² and Ch. Zhang²

Keywords: *thermoplastic composite pipe, finite-element analysis, progressive damage failure, burst resistance, internal pressure*

Experimental tests and numerical studies were performed to investigate the burst performance of thermoplastic composite pipes (TCPs) under internal pressure. A progressive damage model is established to predict the burst behavior of TCPs, in which different failure criteria and the damage evolution of a composite material are considered and directly incorporated into the ABAQUS with a user-defined UMAT subroutine. A series of burst tests on TCPs with different numbers of reinforced layers were carried out, and experimental results were in good agreement with the corresponding numerical predictions. In addition, based on the adaptive progressive damage model, a parametric study into winding angles of TCPs with eight reinforced layers is conducted to evaluate their burst performance.

1. Introduction

Among many composite material structures, thermoplastic composite pipes (TCPs) [1] have gained widespread applications in many fields of ocean engineering owing to their light weight, high corrosion resistance, and good bending performance.

In the process of oil and gas exploitation, the inner pressure of TCPs is variable due to the unstable output status of oil and gas and the rapid expansion of transported liquid when heated. Therefore, the burst failure may occur occasionally during

¹School of Transportation and Civil Engineering, Nantong University, Nantong, 226019, China

²College of Engineering, Ocean University of China, Qingdao, 266100, P. R. China

³Shandong Provincial Key Laboratory of Ocean Engineering, Ocean University of China, Qingdao, 266100, P. R. China

*Corresponding author; tel.: +86 532 66783716; e-mail: shuqing@ouc.edu.cn

a rapid increase in the internal pressure load. However, the damage of composite materials starts as tiny invisible cracks between fibers and the matrix, which degrade the stiffness of composite materials and reduce the load-bearing capacity of TCPs. Consequently, it is important to investigate the burst damage mechanism of TCPs in order to predict their initial damage under an internal pressure, determine the critical burst pressure, and provide some guidance for the design of TCPs.

Many theoretical studies of multilayered filament-wound composite pipes have been performed by various scientists. Xia et al. [2] presented an exact elastic solution for stresses and deformations of pipes under internal pressure based on the three-dimensional (3-D) anisotropic elasticity. The shear-extension coupling was also considered, and different layer stacking sequences of pipes were investigated. In [3], thermal stresses and strains in a filament-wound fiber-reinforced sandwich pipe under a combined internal pressure and thermomechanical loading were analyzed. Bakaiyan et al. [4] studied stress, strain, and deformation distributions in multilayered filament-wound composite pipes with different winding angles under a combined internal pressure and thermomechanical loading. Ansari et al. [5] performed a stress analysis of multilayered filament-wound composite pipes subjected to cyclic internal pressure and thermal loadings. Bai et al. [6] calculated the burst strength of a reinforced thermoplastic pipe using an analytical and FEA approaches and obtained well agreeing results. Onder et al. [7] investigated the influence of temperature and winding angle on the burst pressure of filament-wound composite pressure vessels subjected to an alternating pure internal pressure, and the optimum winding angle was found to be 55°. The majority of investigation results were found by the 3-D anisotropic elasticity theory without considering the progressive damage of composite materials.

Unlike the theoretical studies, several of experimental works have revealed some specific failure mechanisms and failure modes of filament-wound composite pipes. Multiaxial stress tests were performed on filament-wound glass fiber-reinforced epoxy tubes by Meijer and Ellyin [8]. It was found that, at rupture, the fiber structure had been thrust outwards and ends of the fractured fibers were no longer constrained by the matrix. Mertiny et al. [9] conducted an experimental study on the performance of multiangle filament-wound tubes under various stress ratios (axial/hoop). A small reduction in strength was recorded for the tubes in hoop stress-dominated loading conditions.

With development of the finite-element method, some researchers have studied the progressive damage of filament-wound composite pipes and the degradation of material properties by a numerical simulation. A numerical and experimental study was performed by Martins et al. [10] to study the functional and structural failure pressure of composite tubes with different winding angles under an internal pressure. They also investigated the effect of stress ratio and loading conditions on the fracture morphology of filament-wound composite pipes [11]. Rafiee and Amini [12] examined the functional failure pressure of glass-fiber-reinforced polyester pipes under an internal hydrostatic pressure. A progressive modeling procedure based on the rules of sudden stiffness and strength degradation was implemented to predict the critical internal pressure. Based the techniques mentioned above, investigations into the burst behavior of filament-wound composite pipes have been performed actively, but the burst performance of TCPs with an inner liner and outer cover have been addressed less.

The main purpose of our work was to investigate the burst resistance of glass-fiber TCPs under an internal pressure by numerical and experimental methods. TCPs with different number of reinforced layers were manufactured and subjected to burst tests. In addition, a suitable progressive damage model is established to predict the critical burst pressure and failure mechanisms of the composite material. The damage evolution and stiffness degradation of the composite material are simulated numerically using the UMAT subroutine. To verify the applicability of the progressive damage model, experimental results are compared with the numerical predictions. In addition, the effect of different angle-ply reinforced layer systems on the burst performance of TCPs are investigated based on the damage model.

2. Experimental analysis of TCPs

Burst tests of TCPs were carried out to investigate the effect of different numbers of reinforced layers on the critical burst pressure. The tests were run according to ASTM standard 1599-99 “Standard Test Method for Resistance to Short-Time Hydraulic Pressure of Plastic Pipe, Tubing, and Fittings” [13]. During the tests, the critical burst pressures of TCPs and hoop/axial strains were measured.

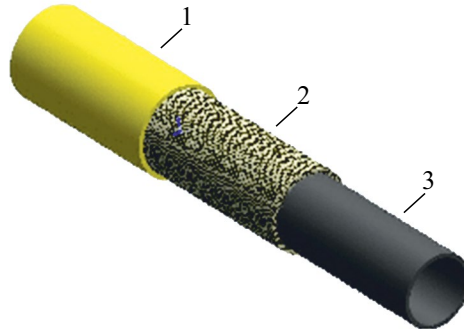


Fig. 1. Classical structure of TCPs: 1 — outer layer, 2 — reinforced layer, and 3 — inner layer.

TABLE 1. Results of Burst Tests

TCPs	Number of layers	Length of pipe, m	Outer diameter, mm	Burst position, L^*	Loading time, s	Actual φ , deg	Burst pressure, MPa	Lay-up configuration
1	4	0.992	61.6	2/5-1/2	59	53.8	24.5	$[\pm 55]_2$
2	6	1.012	62.8	2/5-1/2	59	54.2	34.5	$[\pm 55]_3$
3	8	1.006	64.3	1/5-3/10	62	53.5	43.0	$[\pm 55]_4$
4	10	0.988	64.9	2/5-1/2	68	54.5	50.5	$[\pm 55]_5$
5	12	0.994	66.1	2/5-1/2	64	53.6	57.5	$[\pm 55]_6$

* L is specimen length

2.1. Preparation of TCPs

The main research objects of this paper are glass-fiber thermoplastic composite pipes (TCPs) with winding angles $\varphi = \pm 55^\circ$, an inner diameter of 46 mm, 4-mm-thick inner liner, reinforced middle layers made from 0.25-mm-thick glass-fiber thermoplastic prepreg tapes consisting of high-modulus reinforcing fibers embedded in a low-modulus High-Density Polyethylene (HDPE) matrix, and a 3-mm-thick outer cover, as shown in Fig. 1. The filament winding technology was used to manufacture the reinforced middle layers [14].

In regard to burst tests, the length of TCPs between the end closures should be not less than five times their outer diameter [15]. Therefore, in our experiment, the length of each TCP was 1.0 m. Five kinds of TCPs, with different numbers of reinforced layers, were fabricated, and their detailed parameters are indicated in Table 1. All pipes were inspected, and no clear structure damage was found. The outer diameters and lengths of each TCP were measured several times using a meter ruler, and their average values are also shown in Table 1. It is worth noting that even small changes in the pipe winding angle φ during their manufacture can cause significant calculation errors in a numerical analysis. Therefore, the actual winding angles were measured for each TCP at different places using an appropriate software tool based on the picture of reinforced layers. Their average values are also given in Table 1. Besides, at least three parallel tests were run for each kind of TCP according to the rule for ‘Thermoplastic composite pipes’ [15]. In addition, three strain gages with two measuring directions were placed on the outer surface of each specimen to measure the hoop and axial strains. A schematic of locations of the measuring points is shown in Fig. 2.

2.2. Experimental equipment and process

A pressurizing system was designed to apply a continuously increasing internal hydraulic pressure to the TCPs tested. This system included a gas cylinder, air pump, pressure gage, strain acquisition system, laptop computer, and some protective

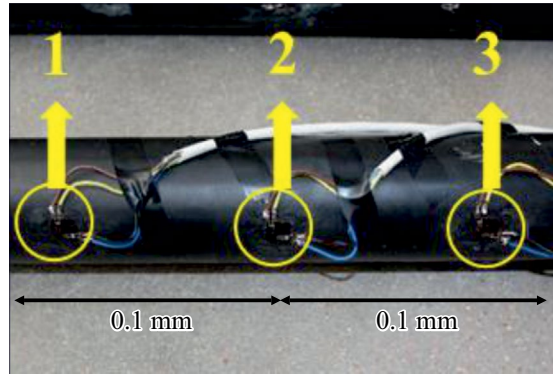


Fig. 2. Locations of measurement points.

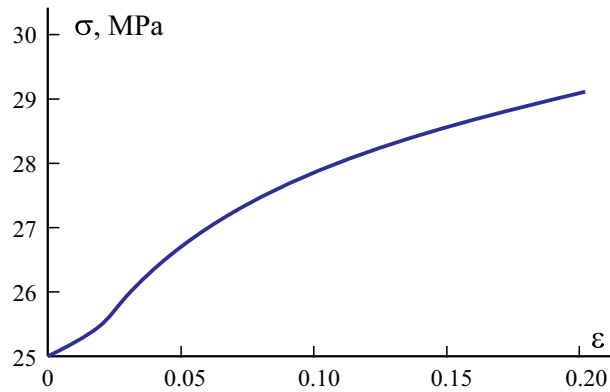


Fig. 3. Stress–strain diagram $\sigma - \varepsilon$ of HDPE.

equipment. The TCPs could freely deform in the radial direction during the loading process. The hoop and axial strains were recorded by a strain acquisition system. Before tests, the specimens were conditioned at a test temperature of $23 \pm 2^\circ\text{C}$ for a minimum of 1 h in a liquid bath or 16 h in a gaseous medium.

At the beginning of burst tests, water was injected into TCPs by the air pump. The change in the internal pressure in TCPs was monitored by a pressure gage. The internal pressure was raised slowly from 0 up to the critical burst pressure, when the TCP burst instantaneously and the pressure dropped quickly to zero. A stop watch was used to measure the pressurization time, which was kept at about 60 s.

2.3. Material properties of HDPE and TCP laminates

As mentioned above, the TCPs were composed of a HDPE and TCP laminates. The elastic modulus of HDPE was 900 MPa and Poisson's ratio 0.38. An isotropic function could be used to input the material property of the HDPE in ABAQUS. The nonlinear stress–strain diagram of HDPE was obtained from a tensile test and is illustrated in Fig. 3. The elastic constants of the transversely isotropic glass-fiber composite laminates were as follows: $E_1 = 28,000$ MPa, $E_2 = E_3 = 3200$ MPa, $\mu_{12} = \mu_{13} = 0.0343$, $G_{12} = G_{13} = 2705$ MPa, $G_{23} = 1230$ MPa, $\sigma_{11}^{f,t} = 829$ MPa, $\sigma_{11}^{f,c} = 146$ MPa, $\sigma_{22}^{f,t} = \sigma_{33}^{f,t} = 30$ MPa, $\sigma_{22}^{f,c} = \sigma_{33}^{f,c} = 49$ MPa, and $\tau_{12}^f = 18$ MPa.



Fig. 4. Fracture morphologies of TCPs with 4 (1), 6 (2), 8 (3), 10 (4), and 12 (5) reinforced inner layers.

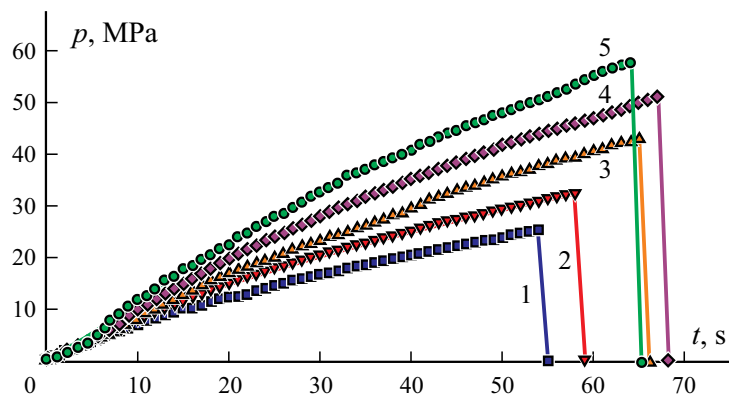


Fig. 5. Internal pressure–time curves $p-t$ of TCPs with 4 (1), 6 (2), 8 (3), 10 (4), and 12 (5) reinforced inner layers.

2.4. Experimental results

The main purpose of the burst tests was to evaluate the ultimate internal pressure of TCPs and to obtain their strain response and fracture morphology. It is worth noting that, in order to ensure the accuracy of the internal pressure tests, the spiral connectors were customized to seal and fix both ends of TCPs, and that the ratio of the biaxial pressure loading (hoop : axial) was 2:1. Different fracture morphologies of TCPs with different numbers of reinforced layers are illustrated in Fig. 4.

As is clearly seen, the fracture morphologies in the burst regions were always oriented along the directions of filament winding, and the damage modes in composite layers were fiber breakage and matrix cracking. In addition, it is noteworthy that the burst positions were always distant from both ends of TCPs, which eliminated the possibility of experimental failure, namely, if burst openings were located at the ends of TCPs, this could be caused by a poor sealing between TCPs and end closures.

The final burst pressures, burst positions on TCPs, and loading times are indicated in Table 1. It is significant that the critical burst pressure increased with number of reinforced layers, and the burst failure positions were located in the middle of TCPs. The internal pressure–time curves are shown in Fig. 5.

3. Numerical simulation of TCPs

The burst behavior of TCPs under internal pressure was also investigated by a numerical simulation. The UMAT user subroutine was used to simulate the progressive damage failure of the composite material (including fiber breakage and matrix cracking). Based on the continuum damage theory, the UMAT was coded with FORTRAN and implemented in the ABAQUS. Besides, the appropriate FE models were created to simulate the failure behavior of TCPs under internal pressure.

3.1. Progressive damage theory

To describe the damage in the fibers and matrix without distinguishing between the tension and compression, the user UMAT subroutine, based on the model proposed by Linde et al. [16], was employed. The failure criteria of matrix and fiber used here are founded on a strain-based continuum damage formulation. The maximum stress, Hoffman, Tsai–Hill, and Tsai–Wu criteria have usually employed to predict the failure strength of composite laminates in the previous studies. A different approach, considering a gradual degradation of stiffness of composite materials controlled by individual fracture energies of the matrix and fiber, was undertaken in [17]. According to this approach, damage in the fiber is initiated when the following criterion is obeyed:

$$f_f = \sqrt{\frac{\varepsilon_{11}^{f,t}}{\varepsilon_{11}^{f,c}} (\varepsilon_{11})^2 + \left(\varepsilon_{11}^{f,t} - \frac{(\varepsilon_{11}^{f,t})^2}{\varepsilon_{11}^{f,c}} \right) \varepsilon_{11}} > \varepsilon_{11}^{f,t} \quad (1)$$

where $\varepsilon_{11}^{f,t} = \sigma_{11}^{f,t} / C_{11}$ and $\varepsilon_{11}^{f,c} = \sigma_{11}^{f,c} / C_{11}$ are the failure strains in the fiber direction in tension and compression, respectively; $\sigma_{11}^{f,t}$, and $\sigma_{11}^{f,c}$ are the longitudinal tensile and compression strengths of the composite material in the TCP; C_{ij} are components of the elasticity matrix in the undamaged state; ε_{ij} ($i, j = 1, 2, 3$) are strains.

When damage criterion (1) is reached, the fiber damage variable d_f is expressed as

$$d_f = 1 - \frac{\varepsilon_{11}^{f,t}}{f_f} \exp \left[-\frac{C_{11} \varepsilon_{11}^{f,t} (f_f - \varepsilon_{11}^{f,t})}{G_f} \right], \quad (2)$$

where G_f is the fracture energy of glass fiber.

Damage in the matrix is initiated when the following criterion is satisfied:

$$f_m = \sqrt{\frac{\varepsilon_{22}^{f,t}}{\varepsilon_{22}^{f,c}} (\varepsilon_{22})^2 + \left(\varepsilon_{22}^{f,t} - \frac{(\varepsilon_{22}^{f,t})^2}{\varepsilon_{22}^{f,c}} \right) \varepsilon_{22} + \frac{\varepsilon_{22}^{f,t}}{\varepsilon_{12}^f} (\varepsilon_{12})^2} > \varepsilon_{22}^{f,t}, \quad (3)$$

where $\varepsilon_{22}^{f,t} = \sigma_{22}^{f,t} / C_{22}$ and $\varepsilon_{22}^{f,c} = \sigma_{22}^{f,c} / C_{22}$ are the tensile and compression failure strains perpendicular to the fiber direction and $\varepsilon_{12}^f = \tau_{12}^f / C_{44}$ is the shear failure strain in the composite material; $\sigma_{22}^{f,t}$, $\sigma_{22}^{f,c}$, and τ_{12}^f are the transverse and shear strengths of the composite material in the TCP.

When damage criterion (3) is satisfied, the fiber damage variable d_m is expressed as

$$d_m = 1 - \frac{\varepsilon_{22}^{f,t}}{f_m} \exp \left[-\frac{C_{22} \varepsilon_{22}^{f,t} (f_m - \varepsilon_{22}^{f,t})}{G_m} \right], \quad (4)$$

where G_m is the fracture energy of matrix.

In our work, the fracture energies of fiber and matrix used in the UMAT were $G_f=12.5$ N/mm and $G_m=1$ N/mm [18], respectively.

After the progressive damage failure, the effective elasticity matrix C is reduced by the damage variables d_f and d_m and takes the form

$$C_d = \begin{bmatrix} (1-d_f)C_{11} & (1-d_f)(1-d_m)C_{12} & (1-d_f)C_{13} & 0 & 0 & 0 \\ & (1-d_m)C_{22} & (1-d_f)(1-d_m)C_{23} & 0 & 0 & 0 \\ & & C_{33} & 0 & 0 & 0 \\ & & & (1-d_f)(1-d_m)C_{44} & 0 & 0 \\ & & & & C_{55} & 0 \\ \text{sym.} & & & & & C_{66} \end{bmatrix}, \quad (5)$$

where the effective elasticity coefficients C_{ij} are expressed in terms of elastic material constants, namely,

$$C_{11} = \frac{1 - \mu_{23}\mu_{32}}{E_2 E_3 \Delta}, \quad C_{12} = \frac{\mu_{21} + \mu_{23}\mu_{31}}{E_1 E_3 \Delta}, \quad C_{13} = \frac{\mu_{31} + \mu_{21}\mu_{32}}{E_1 E_2 \Delta}, \quad C_{23} = \frac{\mu_{32} + \mu_{12}\mu_{31}}{E_1 E_2 \Delta}, \quad (6)$$

$$C_{22} = \frac{1 - \mu_{13}\mu_{31}}{E_1 E_3 \Delta}, \quad C_{33} = \frac{1 - \mu_{21}\mu_{12}}{E_1 E_2 \Delta}, \quad C_{44} = G_{12}, \quad C_{55} = G_{13}, \quad C_{66} = G_{23}.$$

Here, $\Delta = \frac{1 - \mu_{21}\mu_{12} - \mu_{23}\mu_{32} - \mu_{31}\mu_{13} - \mu_{23}\mu_{31}\mu_{12} - \mu_{13}\mu_{32}\mu_{21}}{E_1 E_2 E_3}$, with the subscripts 1, 2, and 3 referring to the

longitudinal, transverse, and radial directions, respectively.

Employing the progressive damage matrix C_d , stresses in the composite structure are updated in the user-defined UMAT subroutine according to the equation

$$\sigma = C_d \varepsilon. \quad (7)$$

The stiffness degradation of a composite material often leads to severe convergence difficulties in such implicit analysis programs as the ABAQUS/Standard software. To improve the convergence, the technique based on the viscous regularization of damage variables is implemented in the user subroutine [18].

In this technique, the damage variables are not calculated from the aforementioned damage evolution directly. Instead, they are “regularized” using the relations

$$\dot{d}_f^v = (d_f - d_f^v) / \eta, \quad \dot{d}_m^v = (d_m - d_m^v) / \eta, \quad (8)$$

where d_f and d_m are the fiber and matrix damage variables calculated according to the damage evolution laws presented above; d_f^v and d_m^v are the “regularized” damage variables used in real calculations of the damage elasticity matrix and the Jacobian matrix; η is the viscosity parameter controlling the rate at which the regularized damage variables d_f^v and d_m^v approach the true damage variables d_f and d_m . In the UMAT user subroutine, the damage variables d_f and d_m are stored as solution-dependent variables SDV1 and SDV2, respectively. Since the numerical results converged rapidly, the viscosity parameter η was taken to be 0.005.

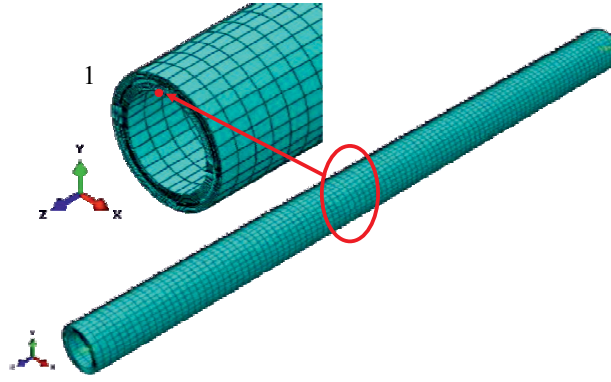


Fig. 6. FE model of a TCP.

3.2. Finite-element model of TCP

In the present paper, the FE model of TCPs is a cylindrical 3D solid element model consisting of three parts: an inner liner, a middle reinforced thermoplastic laminate, and an outer cover.

Ends of the pipe are restrained, and the pipe is loaded by an internal pressure. To consider deformation in the thickness direction, eight-node elements with reduced integration (C3D8R) were selected for TCPs, as shown in Fig. 6. Moreover, the enhanced strain method was adopted to control the hourglass effect for the middle laminate elements. The middle laminates were composed of equal-thickness layers with winding angles of $\pm 55^\circ$.

The ‘Riks method’ was used to capture the static equilibrium states during the unstable phase of structural responses [19]. The basic Riks algorithm is essentially Newton’s method with load magnitude as an additional unknown to find a solution simultaneously for loads and displacements. Thus, the ‘Riks method’ in an analysis procedure that can provide solutions even in the cases of complex and unstable responses.

A mesh convergence analysis was conducted to choose the best mesh size and to determine the computational efficiency. The mesh convergence analysis was performed for seven FE models with different mesh densities in the hoop and axial directions (with 16×60 , 24×80 , 32×100 , 40×120 , 48×140 , 56×160 , and 64×180 elements). All of these models had four reinforced layers with the same winding angle. In the radial direction, the outer cover and the inner liner had eight and six elements respectively. As to the TCP laminate, one element was meshed for each layer. The critical burst pressures in MPa were as follows: 26.13 for 16×60 , 26.73 for 24×80 , 26.83 for 32×100 , 26.85 for 40×120 , 26.89 for 48×140 , 26.90 for 56×160 , and 26.91 for 64×180 meshes. Consequently, each reinforced inner layer was divided into 32×100 elements for a lower computational cost and higher accuracy.

3.3. Numerical results

Based on the FE model mentioned above, five TCP models with different numbers of reinforced layers were calculated to determine their burst resistance. The internal pressure–radial displacement responses $p - \Delta R$ of TCPs with different numbers of reinforced layers were obtained by numerical simulations, and the results are shown in Fig. 7. It can be seen from the figure that the internal pressure rose from 0 up to a maximum and then dropped suddenly when the burst damage of TCP occurred. The critical burst pressure increased with number of reinforced layers in the TCP. From slopes of the $p - \Delta R$ curves in Fig. 7, it can be seen that the stiffness of TCPs grew as the number of reinforced layers increased.

During pressurization, the TCPs underwent three stages of radial deformation until the final destruction occurred. As is seen in Fig. 8, the first stage was from 0 to 5.68 MPa, and then the matrix degradation (SDV2) began. The pressure 5.68 MPa was taken as the matrix failure criterion f_m ($f_m > \varepsilon_{22}^{f,t}$).

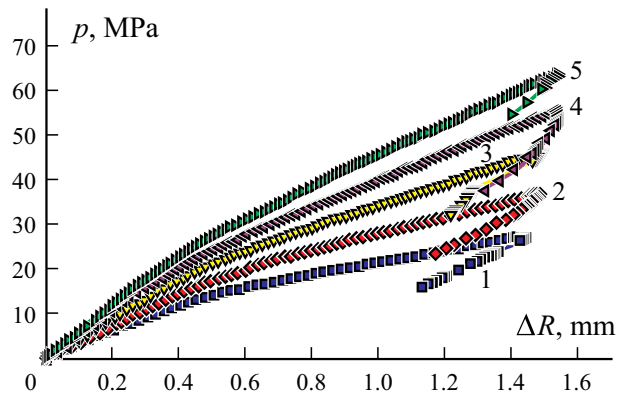


Fig. 7. Internal pressure–radial displacement curves $p-\Delta R$ for TCPs with the nominal winding angle $\varphi = \pm 55^\circ$ and 4 (1), 6 (2), 8 (3), 10 (4), and 12 (5) reinforced inner layers.

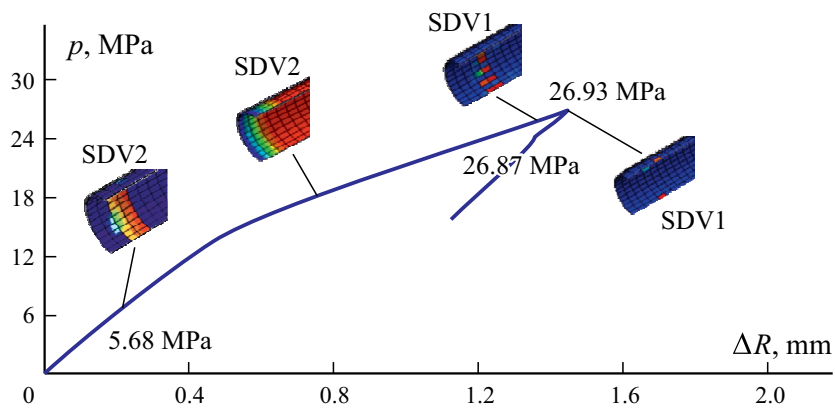


Fig. 8. Stages of radial deformation $\Delta R-p$ of a TCP.

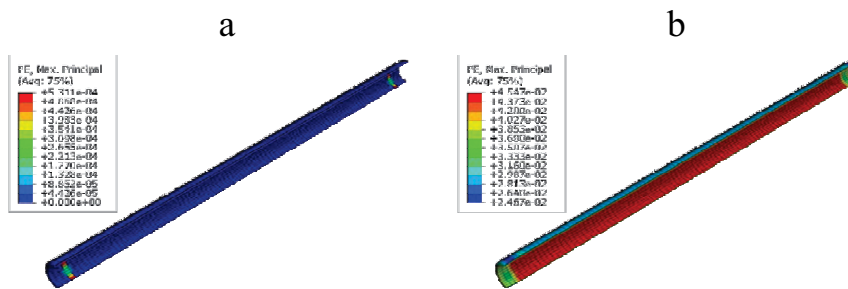


Fig. 9. Distributions of plastic strains in the inner liner at $p = 10.61$ (a) and 25.94 MPa (b).

At the second stage, from 5.68 to 26.87 MPa, the region of matrix cracking gradually expanded until the glass-fiber failure (SDV1) at the inner reinforced layer began. The pressure 26.87 MPa was taken as the fiber failure criterion f_f ($f_f > \varepsilon_{11}^{f,pl}$). It is worth noting that a plastic deformation of the inner liner arose at this stage. As is seen in Fig. 9, when the internal pressure reached 10.61 MPa, plastic deformations occurred at both ends of the pipe, i.e., when the matrix damage arose at 5.68 MPa, the inner liner was still in the elastic region. After the initial plastic deformation of the inner liner, the region of plastic deformation propagated throughout the whole pipe until the pressure reached 25.94 MPa, as illustrated in Fig. 9.

TABLE 2. Critical Burst Pressure of TCPs

TCPs	Number of layers	Experimental results, MPa	Results for the winding angle φ , MPa			
			Nominal	Relation error, %	Actual	Relation error, %
1	4	24.5	26.93	9.92	26.62	8.67
2	6	34.5	36.7	6.38	35.83	3.86
3	8	43.0	45.62	6.09	45.12	4.93
4	10	50.5	55.07	9.05	53.60	6.14
5	12	57.5	63.21	9.93	61.15	6.35

The last stage was from 26.87 to 26.93 MPa. As the internal pressure continued to increase, the initial fiber failure propagated from the inner reinforced layer to the outer reinforced one, and at 26.93 MPa, the fiber fracture arose in the outer reinforced layer, which corresponds to the sharp corner in the displacement–internal pressure curve. At this instant, the TCP have been completely destroyed by the internal critical burst pressure. It is worth mentioning that the critical burst pressure was very close to the pressure causing the initial fiber failure, indicating that, when the fiber of a TCPs exhibits an incipient damage, the eventual destruction of TCP will happen at a slightly higher internal pressure.

4. Comparison of Results

4.1. Critical pressures of TCPs

After the numerical simulation with the UMAT, a comparison between experimental and numerical results was performed to assess the accuracy the of FE model of TCP and the reliability of UMAT for simulating the progressive damage of the composite material. Besides, the critical burst pressures of TCPs with actual winding angles φ were analyzed. The critical burst pressure for actual φ are indicated in Table 2. As is seen, the critical burst pressures of TCPs with the actual φ were slight lower than that of TCPs with the nominal φ . This can be explained by the fact that, for TCPs with smaller φ , the hoop strength decreased.

Table 2 also shows the critical burst pressures obtained from experiments, and they are in good agreement with numerical calculations.

From results for the critical burst pressure, it can be noticed that, because of the large variation in the critical burst pressure at lower winding angles φ , it is necessary to measure the actual winding angles in order to obtain accurate simulation results. For example, the difference in pressure between the nominal and actual φ for the TCP with 12 reinforced layers was 3.58%, as shown in Table 2. Therefore, it is important to measure the actual winding angle of TCPs to avoid overestimation of the critical burst pressure of TCPs and to reduce the difference between numerical simulation and experimental results.

4.2. Comparison of the fracture morphology of TCPs

Figure 4 shows the fracture morphologies of TCPs with different numbers of reinforced layers. At the burst pressure, fibers broke down, the TCPs lost their load-bearing capacity in the hoop direction, and a sudden drop in the internal pressure–radial curve $p - \Delta R$ arose, as shown in Fig. 7.

Figure 10 shows the stress distribution in a failed TCP, which is very similar to the fracture morphology of the TCP in experiments. Both in the experiment and in the numerical simulation, the failure occurred almost in the filament winding direction.

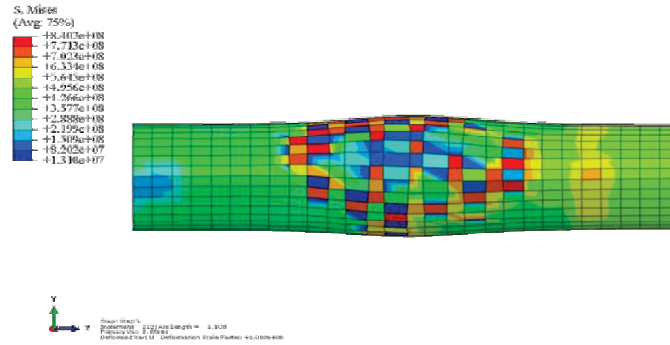


Fig. 10. Stress distribution in a TCP.

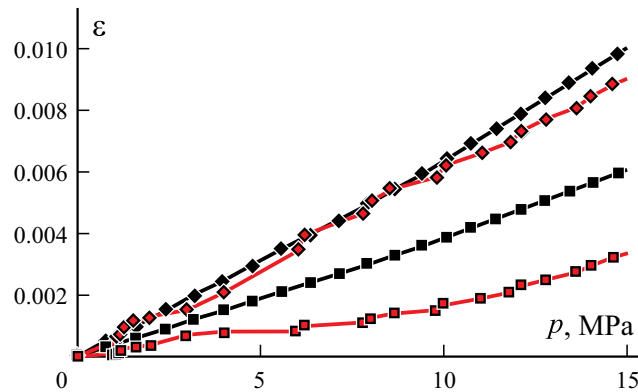


Fig. 11. Internal pressure–strain curves $p - \varepsilon$ in the hoop (1, 2) and axial (3, 4) directions: (1, 3) — FEA and (2, 4) — experimental.

4.3. Strains at the surface of TCPs

As mentioned in the experimental section, a strain acquisition system was used to collect the strains of TCPs in the hoop and axial directions during the pressurization process. The calculated and experimental internal pressure–strain curves of a TCP with eight reinforced layers are illustrated in Fig. 11. It is seen that the results in the hoop direction are in good agreement. However, the difference increased with internal pressure. But the difference between the numerical simulation and experimental results in hoop direction was smaller than in the axial one. This can be explained by the fact that the axial strength of the TCP specimen was higher than in numerical model owing to the longer end closures at both ends of TCP specimen.

5. Effect of Winding Angle φ on the Burst Behavior of TCPs

In most studies, the reinforced layers of TCPs are typically made by filament winding at one certain orientation. The winding angle φ is generally taken to be 54.7° in order to fully utilize the strength properties of the fiber-reinforced layers in TCPs [20]. However, it has been reported that the performance of TCP can be improved using double angle-ply layer systems with different winding angles [21]. Therefore, the influence of double angle-ply reinforced layer systems on their burst performance deserve further investigations. Based on the numerical model mentioned above, the effects of different angle-ply reinforced layer systems on the burst behavior of TCPs are studied in the following.

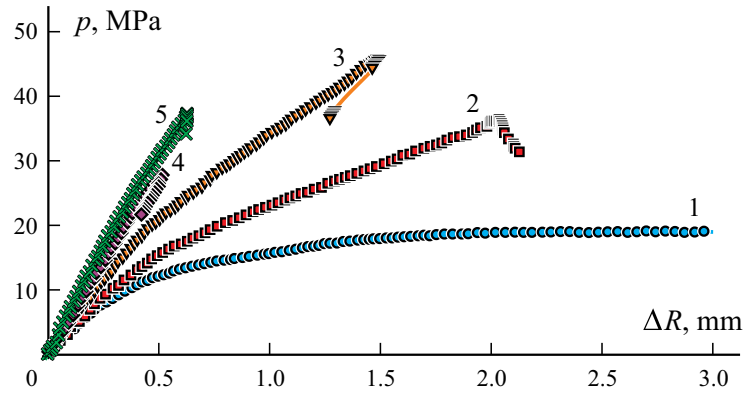


Fig. 12. Internal pressure–radial displacement curves $p - \Delta R$ of TCPs, with winding angles $\varphi = \pm 35$ (1), ± 45 (2), ± 55 (3), ± 65 (4), and $\pm 75^\circ$ (5).

TABLE 3. Different Stacking Sequences of TCPs

No.	Layer sequences	Critical burst pressure, MPa	No.	Layer sequences	Critical burst pressure, MPa
1	$[\pm 75/\pm 75/\pm 55/\pm 55]$	30.67	5	$[\pm 55/\pm 75/\pm 55/\pm 75]$	30.77
2	$[\pm 55/\pm 75/\pm 75/\pm 55]$	31.31	6	$[\pm 55/\pm 75/\pm 75/\pm 75]$	42.44
3	$[\pm 75/\pm 55/\pm 75/\pm 55]$	30.64	7	$[\pm 55/\pm 55/\pm 75/\pm 75]$	48.64
4	$[\pm 75/\pm 55/\pm 55/\pm 75]$	30.58	8	$[\pm 55/\pm 55/\pm 55/\pm 75]$	39.41

5.1. Single angle-ply layer system

TCPs with eight reinforced layers were considered to study the effect of different angle-ply systems on their burst behavior. For five TCP models with different single angle-ply reinforced layer systems ($\varphi = \pm 35, \pm 45, \pm 55, \pm 65$, and $\pm 75^\circ$), the effect of single winding angle φ on their burst behavior was investigated. In numerical simulation, the progressive damage model was used to predict the burst pressure and the progressive damage of TCPs. The internal pressure–radial displacement $p - \Delta R$ histories of different TCPs found from numerical simulation are illustrated in Fig. 12. As is seen at $\varphi = \pm 35$ and $\pm 45^\circ$, the internal pressure–radial displacement curves of TCPs show a flatter trend. This is because that, at smaller winding angles, the strength of TCPs in the hoop direction is lower. At $\varphi = \pm 65$ and $\pm 75^\circ$, slopes of the curves are greater than that at $\varphi = \pm 55^\circ$, and the strength of TCPs in the hoop direction is sufficient to bear a higher internal pressure. But the strength in the axial direction becomes weakened, which can induce matrix cracking in the hoop direction of reinforced layers and reduce resistance of TCP to the internal pressure. At $\varphi = \pm 55^\circ$, the TCP has a higher burst resistance, which agrees with the highest critical burst pressure. The same conclusion has also been made in [7, 10].

5.2. Double angle-ply layer system

To compare the effect of double angle-ply reinforced layer systems on the burst performance of TCPs, the winding angles of $\varphi = \pm 75^\circ$ were also included in them. Eight stacking sequences of double angle-ply reinforced layer systems were analyzed by the finite-element method. Their stacking sequences, from inside to outside (1-8), are indicated in Table 3 together with the critical burst pressures.

As is seen, the system $[\pm 55/\pm 55/\pm 75/\pm 75]$ can take up the highest internal pressure load. This is because that exactly the outside reinforced layers with $\varphi = \pm 75^\circ$ increase most the hoop strength of TCPs.

Thus, it can be concluded that the adjustment of fiber direction is very important for increasing the internal pressure resistance of TCPs. However, in the process of actual manufacture, the fiber winding angle φ can vary, which will affect the final resistance of TCPs to the internal hydrostatic pressure. In order to clear up the effect of errors in the winding angle on the predicted critical pressure of TCPs, Rafiee et al. [22-24] performed a stochastic modeling instead of the deterministic one, considering that the fiber volume fraction, winding angle, and mechanical properties are random parameters. The results obtained confirmed the importance of taking into consideration the manufacturing variability of TCPs.

6. Conclusions

In this work, numerical simulations and burst tests were performed to investigate the burst resistance of glass-fiber TCPs. A progressive damage model of TCPs was established for predicting the critical burst pressure and damage mechanism. The values of pressure causing matrix cracking, plastic deformation, and fiber breakage were determined by numerical simulations.

Burst tests were run on a series of TCPs with different numbers of reinforced layers. The results of experiments and numerical simulations were in a good agreement for all the TCP specimens considered, indicating that the adoptive progressive damage model can be used to predict the burst pressure of TCPs accurately.

Comparing the numerical results for the actual and nominal winding angles φ showed that closer to experimental data were those for the actual φ . Therefore, to predict the critical burst pressure accurately, it is necessary to measure the actual winding angle of TCPs.

With increasing internal pressure, first the matrix cracking occurred, and then the plastic deformation aroused in the inner liner with matrix cracking propagating gradually; after that, the fiber damage began and propagated from the inner to outer reinforced layers, and finally, the TCP broke down. It is worth noting that, after the initial damage of fiber, the failure of TCP occurred soon.

The burst resistance of TCPs with different angle-ply reinforced layer systems were also studied by numerical simulations. The critical burst pressure was found to be sensitive to the angle-ply reinforced layer systems. For the single angle-ply reinforced layer systems, the optimum winding angle was $\pm 55^\circ$. For the double angle-ply reinforced layer systems, the optimum layout was $[\pm 55/\pm 55/\pm 75/\pm 75]$. In summary, it can be asserted that a reasonable layout can effectively improve the bearing capacity of TCPs under an internal pressure. Moreover, the stochastic model of TCPs, which can effectively consider the influence of some random parameters, such as winding angles and the fiber volume fraction should be further investigated.

Acknowledgements. The study was financially supported of the National Science Fund for Distinguished Young Scholars (No.51625902), the Offshore Flexible Pipe Project from Ministry of Industry and Information Technology (No.931648030), and the Taishan Scholars Program of Shandong Province (TS201511016).

REFERENCES

1. URL: <https://airborneoilandgas.com/home> (reference date 18 August 2018).
2. M. Xia, H. Takayanagi, and K. Kemmochi, "Analysis of multi-layered filament-wound composite pipes under internal pressure," *Compos. Struct.*, **53**, No. 4, 483-491 (2001).
3. M. Xia, K. Kemmochi, and H. Takayanagi, "Analysis of filament-wound fiber-reinforced sandwich pipe under combined internal pressure and thermomechanical loading," *Compos. Struct.*, **51**, No. 3, 273-283 (2001).
4. H. Bakaiyan, H. Hosseini, and E. Ameri, "Analysis of multi-layered filament-wound composite pipes under combined internal pressure and thermomechanical loading with thermal variations," *Compos. Struct.*, **88**, No. 4, 532-541 (2008).
5. R. Ansari, F. Alisafaei, and P. Ghaedi, "Dynamic analysis of multi-layered filament-wound composite pipes subjected to cyclic internal pressure and cyclic temperature," *Compos. Struct.*, **92**, No. 5, 1100-1109 (2010).

6. Y. Bai, F. Xu, P. Cheng, M. F. Badaruddin, and M. Ashri, "Burst capacity of reinforced thermoplastic pipe (RTP) under internal pressure," In Proceedings of the International Conference on Offshore Mechanics and Arctic Engineering, **4**, 281-288 (2011).
7. A. Onder, O. Sayman, T. Dogan, and N. Tarakcioglu, "Burst failure load of composite pressure vessels," *Compos. Struct.*, **89**, No. 1, 159-166 (2009).
8. G. Meijer and F. A. Ellyin, "Failure envelope for ± 60 filament wound glass fibre reinforced epoxy tubulars," *Compos. Pt. A-Appl. Sci. Manuf.*, **39**, No. 3, 555-564 (2008).
9. P. Mertiny, F. Ellyin, and A. Hothan, "An experimental investigation on the effect of multi-angle filament winding on the strength of tubular composite structures," *Compos. Sci. Technol.*, **64**, No. 1, 1-9 (2004).
10. L. A. L. Martins, F. L. Bastian, and T. A. Netto, "Structural and functional failure pressure of filament wound composite tubes," *Mater. Des.*, **36**, 779-787 (2012).
11. L. A. L. Martins, F. L. Bastian, and T. A. Netto, "The effect of stress ratio on the fracture morphology of filament wound composite tubes," *Mater. Des.*, **49**, 471-484 (2013).
12. R. Rafiee and A. Amini, "Modeling and experimental evaluation of functional failure pressures in glass fiber reinforced polyester pipes," *Comput. Mater. Sci.*, **96**, 579-588 (2015).
13. ASTM D1599-1999, Standard Test Method for Resistance to Short-Time Hydraulic Pressure of Plastic Pipe, Tubing, and Fittings, USA (2005).
14. K. L. Edwards, "An overview of the technology of fibre-reinforced plastics for design purposes," *Mater. Des.*, **19**, No. 1-2, 1-10 (1998).
15. DNVGL-RP-F119, Thermoplastic composite pipes, (2017).
16. P. Linde, J. Pleitner, H. D. Boer, and C. Carmone, "Modelling and simulation of fibre metal laminates," In ABAQUS Users' conference, (2004).
17. Y. Kim, J.F. Davalos, and E.J. Barbero, "Progressive failure analysis of laminated composite beams," *J. Compos Mater.*, **30**, No. 5, 536-560 (1996).
18. ABAQUS, Analysis user's manual, Version 6.14, (2014).
19. M. J. Clarke and G. J. Hancock, "A study of incremental-iterative strategies for non-linear analyses," *Int. J. Numer. Methods Eng.*, **29**, 1365-1391 (1990).
20. M. W. K. Rosenow, "Wind angle effects in glass fibre-reinforced polyester filament wound pipes," *Composites*, **15**, No. 2, 144-152 (1984).
21. M. A. Ashraf, E. V. Morozov, and K. Shankar, "Flexure analysis of spoolable reinforced thermoplastic pipes for offshore oil and gas applications," *J. Reinf. Plast. Compos.*, **33**, No. 6, 533-542 (2014).
22. R. Rafiee, M. Fakoor, Hesamsadat, and Hadi, "The influence of production inconsistencies on the functional failure of grp pipes." *Steel & Composite Structures an International Journal* (2015).
23. R. Rafiee, F. Reshadi, and S. Eidi, "Stochastic analysis of functional failure pressures in glass fiber reinforced polyester pipes," *Mater. Des.*, **67**, 422-427 (2015).
24. R. Rafiee and M. A. Torabi, "Stochastic prediction of burst pressure in composite pressure vessels," *Compos. Struct.*, **185**, 573-583 (2018).
25. R. Rafiee, M. A. Torabi, and S. Maleki, "Investigating structural failure of a filament-wound composite tube subjected to internal pressure: Experimental and theoretical evaluation," *Polym. Test.*, **67**, 322-330 (2018).